Mon. Not. R. Astron. Soc. **393,** 1041–1053 (2009) doi:10.1111/j.1365-2966.2008.14265.x

# High-energy particle acceleration and production of ultra-high-energy cosmic rays in the giant lobes of Centaurus A

M. J. Hardcastle,[1⋆] C. C. Cheung,[2] I. J. Feain[3] and Ł. Stawarz[4,5]

[1]*School of Physics, Astronomy and Mathematics, University of Hertfordshire, College Lane, Hatfield, Hertfordshire AL10 9AB*
[2]*NASA Goddard Space Flight Center, Astrophysics Science Division, Code 661, Greenbelt, MD, 20771, USA*
[3]*CSIRO Australia Telescope National Facility, PO Box 76, Epping, NSW 1710, Australia*
[4]*Kavli Institute for Particle Astrophysics and Cosmology, Stanford University, Stanford, CA 94305, USA*
[5]*Obserwatorium Astronomiczne, Uniwersytet Jagielloński, ul. Orła 171, PL-30244 Kraków, Poland*

Accepted 2008 November 14. Received 2008 November 4; in original form 2008 August 11



**ABSTRACT**

The nearby radio galaxy Centaurus A is poorly studied at high frequencies with conventional radio telescopes because of its very large angular size, but is one of a very few extragalactic objects to be detected and resolved by the *Wilkinson Microwave Anisotropy Probe* (*WMAP*). We have used the five-year *WMAP* data for Cen A to constrain the high-frequency radio spectra of the 10° giant lobes and to search for spectral changes as a function of position along the lobes. We show that the high-frequency radio spectra of the northern and southern giant lobes are significantly different: the spectrum of the southern lobe steepens monotonically (and is steeper further from the active nucleus) whereas the spectrum of the northern lobe remains consistent with a power law. The inferred differences in the northern and southern giant lobes may be the result of real differences in their high-energy particle acceleration histories, perhaps due to the influence of the northern middle lobe, an intermediate-scale feature which has no detectable southern counterpart. In light of these results, we discuss the prospects for *Fermi Gamma-ray Space Telescope* detections of inverse-Compton emission from the giant lobes and the lobes' possible role in the production of the ultra-high-energy cosmic rays (UHECR) detected by the Pierre Auger Observatory. We show that the possibility of a *Fermi* detection depends sensitively on the physical conditions in the giant lobes, with the northern lobe more likely to be detected, and that any emission observed by *Fermi* is likely to be dominated by photons at the soft end of the *Fermi* energy band. On the other hand, we argue that the estimated conditions in the giant lobes imply that UHECRs can be accelerated there, with a potentially detectable $\gamma$-ray signature at TeV energies.

**Key words:** acceleration of particles – cosmic rays – galaxies: jets – radio continuum: galaxies.

## 1 INTRODUCTION

Centaurus A is the closest radio galaxy to us (we adopt $D = 3.7$ Mpc, the average of five distance indicators in Ferrarese et al. 2007). Its proximity makes it one of the brightest extragalactic radio sources in the sky at low frequencies (only exceeded by Cygnus A; Baars et al. 1977), but it also means that the outer 'giant' double lobes (throughout the paper, we use the nomenclature adopted by Alvarez et al. 2000) subtend an angle of ∼10° on the sky, although their total physical size (∼600 kpc in projection) is not unusually large for a radio galaxy of Cen A's luminosity. The large angular size of the lobes has prevented the type of *spatially resolved*, multifrequency study of their spectral structure that is commonplace for more distant radio galaxies (e.g. Alexander & Leahy 1987). While detailed low-frequency maps of the giant lobes have been available for many years (e.g. Cooper, Price & Cole 1965), published radio data from ground-based observations only exist up to 5 GHz (Junkes et al. 1993) and the spectral study of Alvarez et al. (2000), involving (at many frequencies) painstaking graphical integration of contour maps, was only able to determine overall spectra for the giant lobes, finding no evidence for deviation from a single power law between 408 MHz and 5 GHz. The low-frequency two-point spectral index maps of Combi & Romero (1997), however, do show some evidence for position-dependent spectral steepening, particularly towards the end of the southern giant lobe.

⋆E-mail: m.j.hardcastle@herts.ac.uk

Cen A is widely believed to be a restarting radio galaxy, in the sense that the inner lobes are the result of the current nuclear activity, while the giant outer lobes are the result of a previous outburst (Morganti et al. 1999). This picture is supported by the observation of hot thermal X-ray emission, apparently the result of strong shocks, surrounding both inner lobes (Kraft et al. 2003, 2007; Croston et al., in preparation) which implies that they are propagating supersonically into the intergalactic medium (IGM) of Cen A and are disconnected from the giant lobes. However, the nature of the intermediate-scale northern middle lobe (NML; Morganti et al. 1999) is not completely clear in this model. In standard spectral ageing models (e.g. Jaffe & Perola 1973), we might expect to see spectral steepening at high frequencies in the giant lobes; a measurement of spectral ageing gives a model-dependent constraint on the time since the last injection of high-energy electrons into these lobes. Such a constraint on spectral age could be compared with other estimates of the dynamical age of the radio source, and would therefore be of considerable interest, but the work of Alvarez et al. (2000) only sets upper limits on this quantity, since they do not see any deviation from a power-law spectrum.

The giant lobes of Cen A are also interesting because they are predicted to be strong sources of inverse-Compton emission as the relativistic electrons in the lobes scatter cosmic microwave background (CMB) photons to high energies; a detection of inverse-Compton emission from Cen A would constrain the magnetic field strength in the lobes of Fanaroff & Riley (1974) class I (hereafter FRI) radio sources in general: we have little information on the magnetic field strengths in these low-power radio galaxies at present. However, X-ray emission from this process would be distributed on similar scales to the giant lobes, making it hard to detect. Cooke, Lawrence & Perola (1978) claimed an early detection of the giant lobes using *Ariel V*, but Marshall & Clark (1981) argued that this was the result of point-source contamination, placing a much lower upper limit on the flux from *SAS 3* observations. At soft X-ray energies (e.g. Arp 1994), the situation is seriously confused by the presence of known thermal X-ray emission from the interstellar medium of the host galaxy, which more recently has been extensively studied with *Chandra* and *XMM–Newton* (e.g. Kraft et al. 2003), and is also hard to study because the X-ray emission fills the field of view of modern soft X-ray imaging instruments such as *ROSAT* (Arp 1994), *XMM* and *ASCA* (Isobe et al. 2001), presenting almost insuperable problems of background modelling and subtraction. However, the spectrum of the inverse-Compton emission should be hard up to high energies (exactly how high depends on the model adopted for the electron energy spectrum, as we will discuss below). There are thus also interesting constraints from observations at MeV to GeV energies made with the *Compton Gamma-ray Observatory* (*CGRO*) (e.g. Steinle et al. 1998; Sreekumar et al. 1999), which do not detect the giant lobes but again set upper limits on their high-energy flux densities. More sensitive hard X-ray/$\gamma$-ray observations exist with wide-field instruments like *INTEGRAL* (e.g. Rothschild et al. 2006) and the *Swift* Burst Alert Telescope (e.g. Markwardt et al. 2005) but as these are coded-aperture instruments they have limited sensitivity to extended emission (see e.g. Renaud et al. 2006). At present, therefore, there is no unambiguous detection of X-ray or $\gamma$-ray inverse-Compton emission from the giant lobes of Cen A. One of us has shown (Cheung 2007) that *Fermi*[1] may have the sensitivity to detect inverse-Compton emission off the CMB from the lobes of Cen A at energies from $\sim$100 MeV to 10 GeV. However, the details of this depend on modelling of the electron energy spectrum at high energies, which in turn depends on high-frequency radio data.

Finally, Cen A's giant lobes are possible sources of ultra-high-energy cosmic rays (UHECRs). Cen A's proximity means that all aspects of the active galaxy – central AGN, inner jets and lobes, and giant lobes – have long been considered as possible UHECR accelerators (see e.g. Cavallo 1978; Romero et al. 1996, and, more recently, Gureev & Troitsky 2008 and references therein). Interest in Cen A has been spurred by the remarkable discovery that two of the 27 UHECR events detected so far by the Pierre Auger Observatory (PAO; Abraham et al. 2007) appear to be arriving from the direction of the centre of Cen A, while at least two additional events may be associated with it (e.g. Wibig & Wolfendale 2007; Fargion 2008; Gorbunov et al. 2008a) due to the large angular extent of the giant radio lobes (Gorbunov et al. 2008b; Moskalenko et al. 2008). Most scenarios discussed in the literature to date assume that UHECRs are produced near the supermassive black hole (SMBH) or in the inner jets (e.g. Cuoco & Hannestad 2008; Kachelriess, Ostapchenko & Tomas 2008), but an explanation in terms of the giant lobes has the advantage that it can easily account for the PAO events seen on larger scales. In order to investigate this quantitatively, we need information about the magnetic field strengths and the *leptonic* particle acceleration in these lobes, which can be provided by a combination of high-frequency radio observations and inverse-Compton constraints or measurements.

The *Wilkinson Microwave Anisotropy Probe* (*WMAP*) has observed the whole sky at frequencies around 20, 30, 40, 60 and 90 GHz (known as *K, Ka, Q, V* and *W* bands, respectively) with the aim of measuring structure in the CMB (e.g. Hinshaw et al. 2008). The currently available *WMAP* data represent 5 yr of observations. Cen A is clearly detected, and spatially resolved, in the *WMAP* observations at all frequencies (e.g. Page et al. 2007) and Israel et al. (2008) have recently presented *WMAP*-derived measurements of the flux density of the whole source, showing that there is clear steepening in the integrated spectrum at high frequencies. Thus, the data are available to carry out a study of the variation of the radio spectrum as a function of position, to fit spectral ageing models to the large-scale lobes and investigate whether we can learn anything about the source dynamics, and to make predictions of the expected inverse-Compton emission from the giant lobes.

In this paper, we present the results of such a study. We first combine the 5-yr *WMAP* data on Cen A with single-dish radio images at lower frequencies to make spatially resolved measurements of the radio spectra from 408 MHz to 90 GHz. We then discuss the implications of the high-frequency detections for the dynamics of Cen A, for possible inverse-Compton detections of the giant lobes at high energies and for acceleration of UHECRs and their possible $\gamma$-ray emission signatures.

## 2 DATA

### 2.1 Radio data

We obtained electronic versions of ground-based radio maps of Cen A to provide low-frequency counterparts to the five *WMAP* images. At 408 MHz, we used the all-sky map of Haslam et al. (1982), which is available from the National Center for Supercomputing Applications Astronomy Digital Image Library.[2] The 1.4-GHz and

[1] Formerly known as the *Gamma-ray Large Area Space Telescope* (*GLAST*).

[2] See http://adil.ncsa.uiuc.edu/document/95.CH.01.01.

4.75-GHz (hereafter, 5-GHz) data were taken with the Parkes telescope and kindly provided to us by Norbert Junkes; the 5-GHz data are those presented by Junkes et al. (1993).

### 2.2 *WMAP* data and processing

Electronic maps of the 5-yr *WMAP* data for Cen A at all five *WMAP* frequencies were kindly provided by N. Odegard. For each map, a monopole defined outside of the *WMAP* Kp2 mask (see e.g. Hinshaw et al. 2007) and the internal linear combination (ILC) CMB map were subtracted. The data were interpolated from HEALPix to a Galactic coordinate grid with 0.°1 spacing. The images were then converted into a celestial coordinate frame using AIPS, and the units of the maps converted from mK to Jy beam$^{-1}$ for ease of comparison with the ground-based radio maps, which have these units. For the unit conversion, we used the beam areas tabulated by Page et al. (2003) and added a 'beam size' header to the file that defined the beam to be a Gaussian of the same area. Although the *WMAP* beam is not a Gaussian (Page et al.), this approximation has no effect on our flux density measurements, since the two identical values of beam area cancel; in addition, the Gaussian full width at half-maximum (FWHM) of the beam calculated in this way is similar to the true FWHM tabulated by Page et al. (2003), and so gives us a convenient way to characterize the resolution of the resulting maps. We were then able to use AIPS for a simple analysis of the *WMAP* data and software based on the FUNTOOLS package[3] for measurement of flux densities from matched regions of the ground-based and *WMAP* radio maps. The effective central frequencies of the *WMAP* bands for extended emission with a spectral index of 0.7 are 22.5, 32.7, 40.4, 60.1 and 92.9 GHz (based on the bandpass characterization of Jarosik et al. 2003), and we treat measured flux densities as being measured at these central frequencies in all subsequent analysis, although for simplicity we will refer to the different bands as the 20-, 30-, 40-, 60- and 90-GHz bands in what follows.

In measuring flux densities from regions of Cen A with *WMAP* we need to take careful account of the foreground and background characteristics of the data. First, the ILC subtraction described above only takes account of structure in the CMB on scales greater than 1°: this gives rise to real structure on small scales in the maps of this 10° source, which is a problem at higher frequencies and correspondingly high resolutions. Secondly, synchrotron emission from the Milky Way provides a foreground which is both position- and frequency-dependent, being strongest at low frequencies and towards the south of the Cen A field (e.g. de Oliviera-Costa et al. 2008).

For our analysis, we convolved all the images with a Gaussian that gave us approximately the resolution of the 20-GHz *WMAP* image (0.°83) at all observing frequencies, with the exception of the 20-GHz data themselves and of the 408-MHz data set, which already has a very similar intrinsic resolution. The convolution has two effects on our analysis: for the *WMAP* data, it helps to reduce any contamination from the unsubtracted real structure in the CMB, and for all the data sets it allows us to measure flux densities from extended regions with sufficient confidence that we see the same structures at different frequencies.

Fig. 1 shows a montage of the radio images used in this paper. Full-resolution *WMAP* images are presented by Israel et al. (2008).

[3] Documented at http://hea-www.harvard.edu/saord/funtools/ (see also Mandel, Murray & Roll 2001).

## 3 RESULTS

### 3.1 Spectral index mapping

To search for evidence for spectral differences in the large-scale structure of Cen A as a function of position, we initially constructed a map of the two-point spectral index [$\alpha = -\log(S_1/S_2)/\log(\nu_1/\nu_2)$] between 1.4 and 30 GHz (Fig. 2). Such a map can only be approximate given that the beams of the ground-based and *WMAP* data are only approximately matched, and it cannot take account of the varying position-dependent background in the *WMAP* images, but it does provide an indication of whether the spectral steepening already observed by Israel et al. (2008) is position-dependent. The spectral index map gives a strong indication that the spectral index does indeed steepen as a function of distance from the 'nucleus' (which at this resolution includes the entire inner lobe and north middle lobe structures as well as the flat-spectrum core), confirming the lower-frequency (0.4–1.4 GHz) results of Combi & Romero (1997).

### 3.2 Flux density measurements

To investigate spectral changes in the giant lobes more quantitatively, we next divided the radio source into five regions encompassing all the structures detected at 20 GHz. These regions are shown in Fig. 3 and for simplicity we number them 1–5 from north to south on the source. Regions 1 and 2 are, respectively, the outer and inner regions of the northern giant lobe, region 3 is dominated by the emission from the nucleus, inner lobes and north middle lobe, and regions 4 and 5 are, respectively, the inner and outer regions of the southern giant lobe. The regions are all substantially larger than the adopted *WMAP* beam sizes. For each region, we defined two background regions lying adjacent to the source regions in the east–west direction. The background regions were used both to find a mean background flux density, which was subtracted from the total in the source regions (thus removing contamination from our own Galaxy, whose strength varies with position on the maps) and to determine an off-source rms for each map, from which we estimated the on-source noise. Flux measurements and background subtraction were carried out in the same way for all the ground-based and *WMAP* data sets. The measurements of flux density for each region and frequency, together with the error estimated from the background region rms, are tabulated in Table 1 and plotted together in Fig. 4.

We initially note that the total flux density listed in Table 1, the sum of all measured flux densities from the regions, agrees well with the values tabulated by Israel et al. (2008) (their table 1) within the uncertainties. Our flux densities are generally slightly lower, and the discrepancy is greatest at the higher frequencies where we have not attempted to measure fluxes for the whole source, but even here the differences do not exceed the errors quoted by Israel et al. (larger than ours because they do not restrict themselves to regions where emission is clearly detected). The agreement between the two independent analyses strengthens the case that the flux density measurements are correct. We confirm the spectral steepening of the integrated source spectrum detected by Israel et al.

Examination of the spectral energy distributions (SEDs) for individual regions (Fig. 4) shows clear differences between the northern giant lobe (regions 1 and 2), the central region (3) and the southern giant lobe (4 and 5). The central region shows no evidence for spectral steepening except between 5 and 20 GHz. At *WMAP* frequencies, the spectral index $\alpha$ is very consistently about 0.65, close

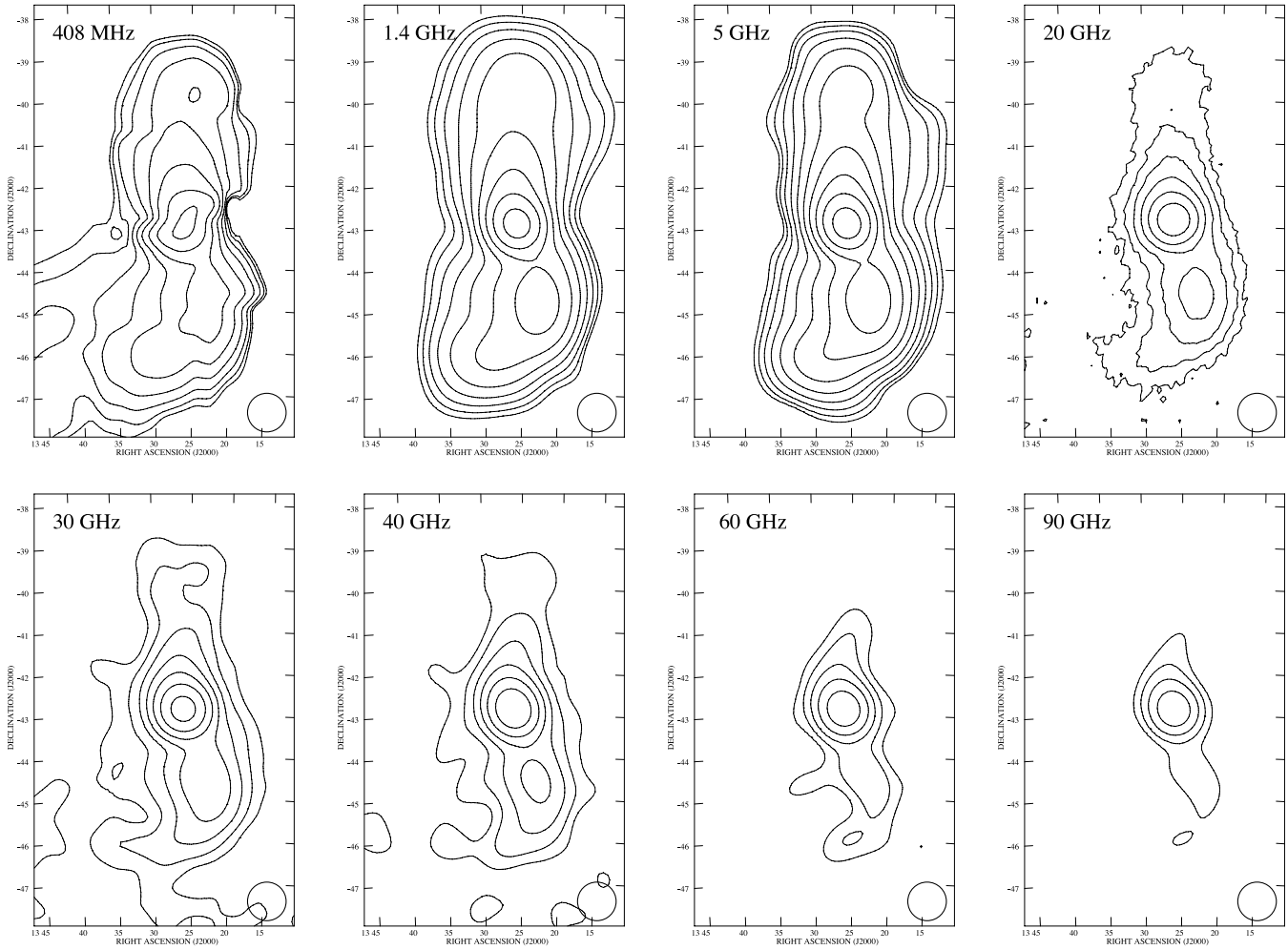


**Figure 1.** Large-scale structure of Centaurus A with a resolution of $\sim 0.^{\circ}83$. Contours are at 1, 2, 4... times the base level specified for each map, and take no account of background, except for the 408-MHz map, from which a constant background of 43 Jy beam$^{-1}$ has been subtracted. Top row, from left- to right-hand side: 408 MHz (3 Jy beam$^{-1}$), 1.4 GHz (1 Jy beam$^{-1}$), 5 GHz (0.25 Jy beam$^{-1}$), 20 GHz (1.0 Jy beam$^{-1}$). Bottom row, from left- to right-hand side: 30 GHz (0.5 Jy beam$^{-1}$), 40 GHz (1.0 Jy beam$^{-1}$), 60 GHz (1.0 Jy beam$^{-1}$), 90 GHz (2.0 Jy beam$^{-1}$). Circles in the bottom right-hand corner of each image indicate the beam size (diameter shows FWHM). The 20-GHz data have different noise characteristics from the other *WMAP* images because they have not been convolved with a Gaussian; instrumental noise on scales smaller than the effective beam is therefore visible. See the text (Section 2.2) for discussion of the convolution, effective resolution and beam area of these images.

to the lower-frequency spectral index of 0.70 derived for the inner lobes by Alvarez et al. (2000). Given that the central region (region 3) in our analysis includes the flat-spectrum core (which is strongly variable; e.g. Israel et al. 2008), the inner lobes, the north middle lobe and some extended lobe emission, it is not surprising that its spectrum is poorly fitted by a single power law or curved spectrum. Probably, it consists of (at least) a flat-spectrum component and a component with a spectral turnover between 5 and 20 GHz.

The spectra of the southern giant lobe regions (regions 4 and 5) remain relatively flat up to 5 GHz, but show clear steepening at high frequencies. Moreover, the spectrum of region 5 (the southern half of the southern giant lobe) is systematically steeper than that of region 4 (the northern half), even at low frequencies (as indicated by our spectral index mapping and also seen by Combi & Romero 1997). This difference is statistically significant: considering just the spectral indices between 1.4 and 5 GHz, $\alpha_4 = 0.55 \pm 0.02$ while $\alpha_5 = 0.71 \pm 0.05$. The systematic increase in spectral curvature as a function of frequency, seen particularly in region 4 (northern south giant lobe), is characteristic of spectral ageing models, and we explore fits of such models to the data below.

On the other hand, the northern giant lobe regions (regions 1 and 2) show no significant spectral differences. Their spectra both start to steepen between 1.4 and 5 GHz and then remain roughly constant (at around $\alpha = 1.0$) at higher frequencies. These spectra are clearly different from those of the southern giant lobe. It does not seem possible to explain this difference in terms of inadequate background subtraction; the Galactic background that we subtract off is a power law, so that it is hard to see how any combination of partially subtracted background and source could produce the differences in the northern and southern regions. The statistical differences (given our adopted errors) between the northern and southern giant lobes are highly significant at both low and high frequencies. We explore the reasons for this difference below (Section 5).

### 3.3 High-resolution imaging of the NML

Finally, we note that in the 90-GHz *WMAP* image, the only one to have the required resolution to distinguish between the inner lobes and the NML, there is a clear extension of the central point source (Fig. 5) which is exactly coincident with the NML. Its flux

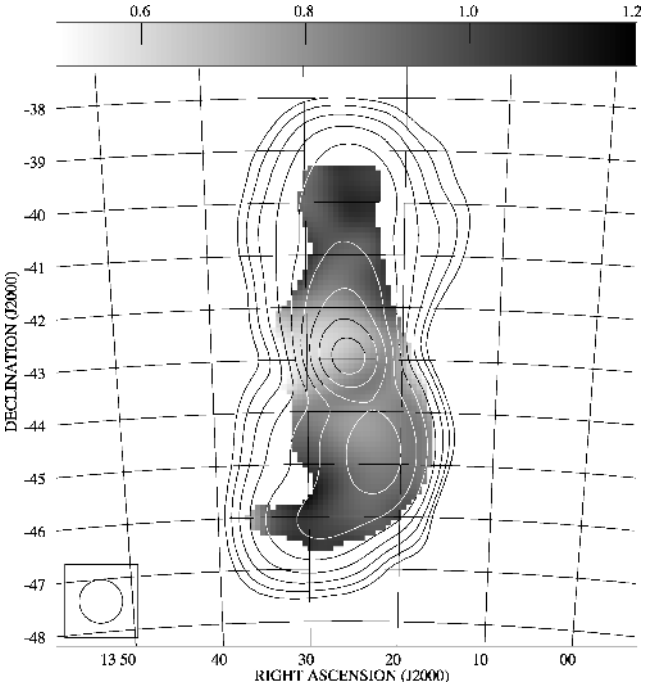


**Figure 2.** Map of two-point spectral index $\alpha$ between 1.4 and 30 GHz in the giant lobes of Cen A. Only pixels where the total intensity exceeds five times the off-source rms level are plotted. Contours are from the 1.4-GHz Parkes data at 1, 2, 4 ... Jy beam$^{-1}$. The resolution (0.°83) is indicated by the circle in the bottom left-hand corner.

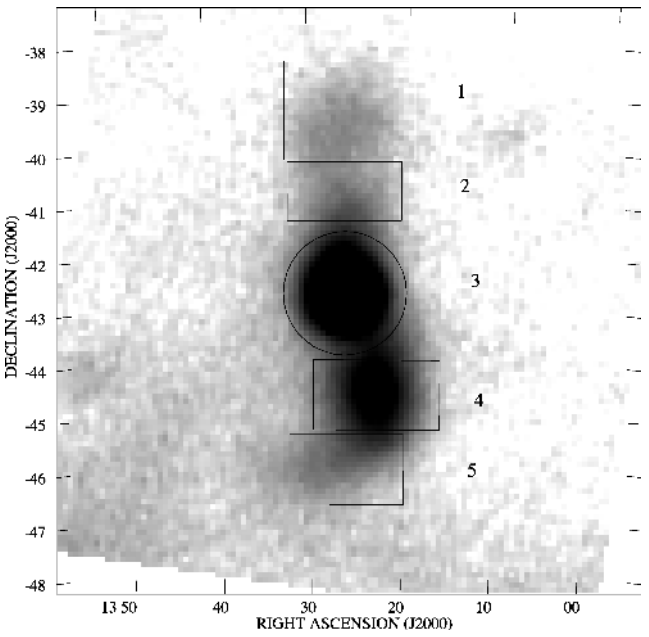


**Figure 3.** Spectral extraction regions used for Table 1 and Fig. 4. The grey-scale shows the 20-GHz *WMAP* data.

density at 90 GHz is around 1.5 Jy which implies a comparatively flat spectrum ($\alpha \approx 0.6$) between 5 and 90 GHz, measuring flux from matched regions of the full-resolution 5-GHz map of Junkes et al. (1993) and the 90-GHz *WMAP* image. This strongly suggests that particle acceleration is either ongoing there or has recently ceased, although given that we only have two spectral data points we cannot rule out the possibility that the spectrum is flatter simply due to a higher magnetic field strength (cf. Katz-Stone, Rudnick & Anderson 1993). We discuss the implications for the nature of the NML in Section 4.

## 4 THE NATURE OF THE NML

As discussed in Section 1, the NML (e.g. Morganti et al. 1999) is a feature at the base of the northern giant lobe, peaking at around 0.°5 (30 kpc in projection) from the active nucleus, that has no counterpart on the southern side. High-resolution radio data (e.g. Junkes et al. 1993; Fig. 5) show a high-surface-brightness feature, centred at around RA = $13^{\rm h}27^{\rm m}$ Dec. = $-42^\circ40'$, which extends smoothly northwards into the larger-scale lobe, with the magnetic field vectors oriented along the long axis of the structure (Junkes et al. 1993). At higher resolutions, still the brightest part of the NML has been imaged by Morganti et al. (1999), who see a jet-like structure (the 'large-scale jet') connecting the NML and the northern inner lobe. Although high-resolution imaging of the northern inner lobe (e.g. Clarke, Burns & Norman 1992) shows a sharply bounded radio structure with no evidence for continued outflow, it is possible (as argued by Morganti et al.) that the existence of the large-scale jet implies that there is continued energy supply to the NML. This interpretation would be consistent with the flat spectrum between 5 and 90 GHz of the base of the NML region (see above). It would also be consistent with the detection of X-ray emission apparently embedded in the lobes (Feigelson et al. 1981; Morganti et al. 1999) which is shown by *XMM* observations to be highly overpressured thermal material, plausibly requiring an interaction with an ongoing outflow (Kraft et al. 2009). The NML is a highly complex region associated with optical filaments and kinematically disturbed neutral hydrogen (Morganti et al. 1999; Oosterloo & Morganti 2005) and any interpretation is difficult, particularly as we are not aware of analogous structures in other restarting sources (Section 1). However, our data support the idea that the NML is, or at least was until recently, fed by an active jet. Assuming an equipartition magnetic field,[4] an 'injection index' (i.e. the synchrotron spectral index of the low-energy electron population) of $\alpha = 0.5$ and a Jaffe & Perola (1973; hereafter J–P) ageing spectrum, the data require particle acceleration to have ceased no more than $7 \times 10^6$ yr ago.

## 5 SPECTRA AND SPECTRAL AGEING IN THE GIANT LOBES

As shown above, the spectra of the giant lobes of Cen A present a mixed picture. The southern giant lobe has a steep high-frequency spectrum and (within the limitations of our data) the spectra appear to steepen systematically both with frequency and with distance from the nucleus (Figs 2 and 4). In the northern giant lobe, the spectra seem very uniform as a function of position and do not steepen significantly with frequency above 5 GHz. What causes these differences in the two giant lobes?

We begin by noting that, given the large integration regions, the southern giant lobe spectra are remarkably well fitted by standard J–P aged synchrotron spectra with an injection index of $\alpha = 0.5$

[4] Here and throughout the paper, except where otherwise stated, we assume an electron–positron plasma with no significant energetic contribution from protons.

**Table 1.** Flux densities of the regions of Cen A as a function of frequency. The final column gives the sum of all measured quantities in the preceding columns. Blanks indicate combinations of frequency and region where significant emission was not visible by eye.

| Frequency | Flux density (Jy) | | | | | |
|---|---|---|---|---|---|---|
| (GHz) | Region 1 | Region 2 | Region 3 | Region 4 | Region 5 | Total |
| 0.408 | 191.3 ± 10.8 | 165.3 ± 12.0 | 1074.0 ± 18.8 | 366.3 ± 26.7 | 238.5 ± 30.7 | 2035.2 ± 47.6 |
| 1.4 | 91.2 ± 2.1 | 74.6 ± 3.0 | 545.0 ± 1.3 | 204.7 ± 4.3 | 111.2 ± 6.0 | 1026.7 ± 8.3 |
| 4.75 | 30.3 ± 0.3 | 26.3 ± 0.9 | 273.5 ± 1.0 | 104.3 ± 0.9 | 47.0 ± 1.7 | 481.4 ± 2.4 |
| 22.5 | 5.7 ± 0.5 | 4.9 ± 0.3 | 71.3 ± 0.6 | 19.6 ± 0.6 | 6.3 ± 0.7 | 107.9 ± 1.2 |
| 32.7 | 4.2 ± 0.4 | 3.4 ± 0.3 | 56.4 ± 0.4 | 13.5 ± 0.4 | 3.9 ± 0.5 | 81.3 ± 0.9 |
| 40.4 | 3.5 ± 0.5 | 2.8 ± 0.4 | 48.8 ± 0.5 | 10.2 ± 0.3 | 3.0 ± 0.5 | 68.3 ± 1.0 |
| 60.1 | – | – | 37.0 ± 0.8 | 5.2 ± 0.6 | 2.2 ± 0.8 | 44.3 ± 1.3 |
| 92.9 | – | – | 28.1 ± 1.9 | – | – | 28.1 ± 1.9 |

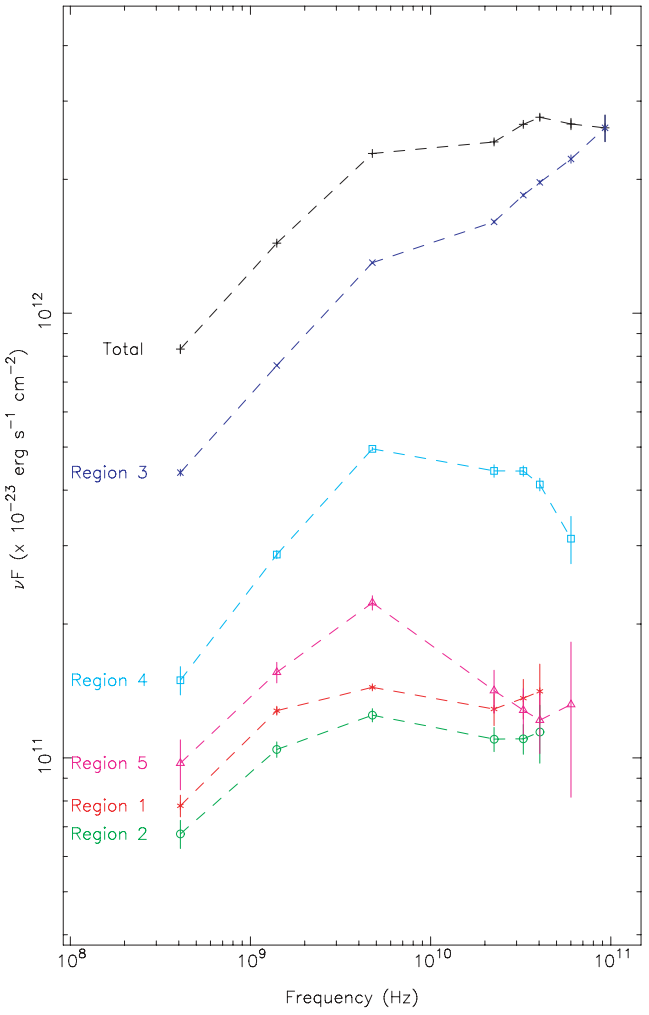


**Figure 4.** Flux density × frequency ($\nu f_\nu$) for the regions of Table 1 (see Fig. 3) as a function of frequency. 1 Jy Hz is $10^{-23}$ erg s$^{-1}$ cm$^{-2}$.

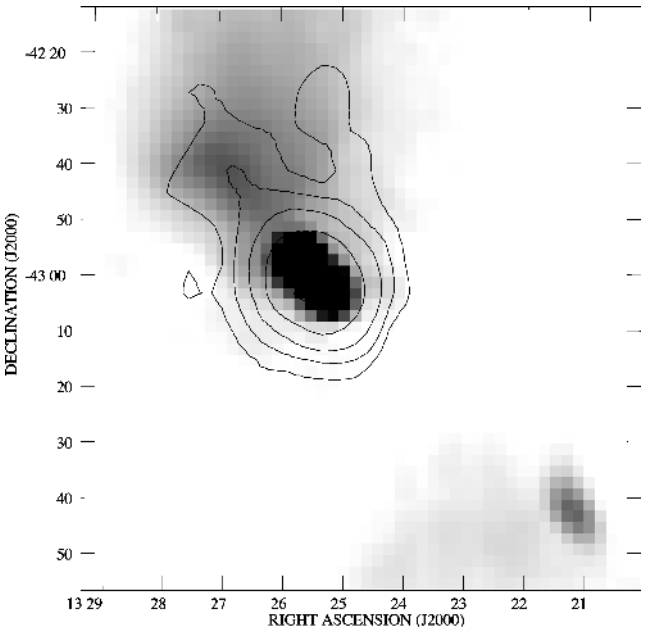


**Figure 5.** *WMAP* and radio images of the central parts of Cen A, showing the elongated structure that we associate with the NML. Contours are from the full-resolution *WMAP* 90-GHz image, at 0.75 × (1, 2, 4. . .) Jy beam$^{-1}$, overlaid on the 5-GHz radio map of Junkes et al. (1993). The area of the *WMAP* beam at this frequency corresponds to an effective resolution around 15 arcmin. The compact feature to the SW of the inner lobes/core of Cen A, undetected at 90 GHz, is a background radio galaxy.

(determined from the low-frequency spectral index).[5] We estimate an equipartition field strength in the integration regions around 1.3 μG (treating them as cylinders in the plane of the sky), which implies that inverse-Compton losses dominate, since the CMB has an energy density equivalent to a magnetic field with a strength of 3.3 μG. If we assume that the field strength has the equipartition values and that the CMB is the dominant photon field, the spectral fits (see Fig. 6 for an example) imply spectral ages of $(2.4 \pm 0.1) \times 10^7$ yr for region 4 and $(2.9 \pm 0.1) \times 10^7$ yr for region 5 (errors are $1\sigma$ statistical errors for one interesting parameter only: systematic errors are dominated by the choice of injection index and ageing field strength). By contrast, regions 1 and 2 (corresponding to the northern giant lobe) are rather poorly fitted by such models, since their low-frequency spectra are too steep and their high-frequency spectra too flat. They are better fitted with standard 'continuous injection' broken power-law models with an injection index of 0.5 steepening to 1.0 at high frequencies (Heavens & Meisenheimer 1987). If a J–P model is fitted, the derived ages are, unsurprisingly,

[5] We note that the injection indices we assume are significantly flatter than the spectral index of the inner lobes measured by Alvarez et al. This is not necessarily a problem, since (1) the equipartition magnetic field strength in the inner lobes is much higher and (2) there is no particular reason to believe that the particle acceleration process currently operating in the inner lobes is the same as that which operated in the giant lobes.

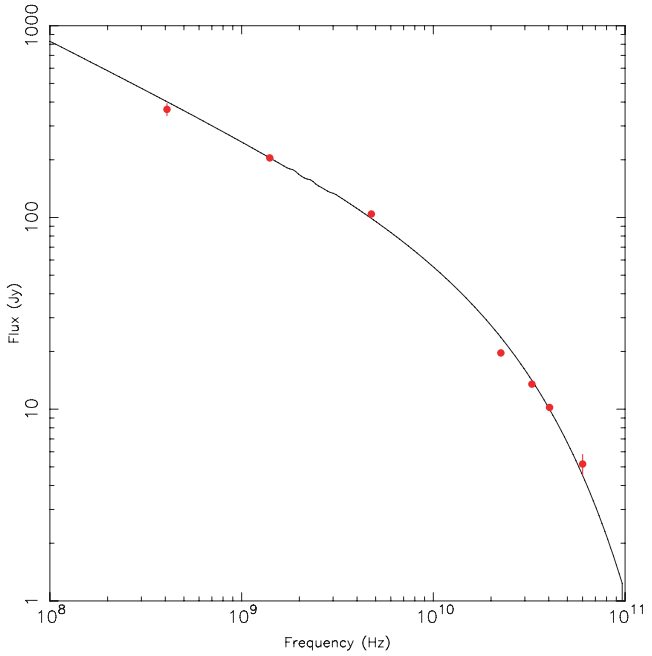


**Figure 6.** Flux densities for region 4 (Table 1) fitted with a standard Jaffe–Perola (1973) aged synchrotron spectrum assuming an injection index (low-frequency spectral index) of 0.5, an ageing $B$-field of 1.3 μG and a spectral age of $2.4 \times 10^7$ yr.

of the same order of magnitude but, implausibly, region 2 appears older than region 1 [ages $(2.1 \pm 0.1) \times 10^7$ and $(2.9 \pm 0.1) \times 10^7$ yr for regions 1 and 2, respectively, where we derive the age uncertainties by rescaling the errors on the data points so as to make the reduced $\chi^2$ of the fit equal to 1]. The ages we derive are similar to the upper limits quoted by Alvarez et al. (2000), who used somewhat lower magnetic field strengths.

One possible explanation for the spectral differences between the two giant lobes is that the northern lobe has undergone some particle injection event that the southern lobe has not. A natural explanation is that this is connected to the existence of the NML (Section 4); in this model, the NML would be currently (or very recently) connected to the energy supply and injecting high-energy electrons into the base of the giant lobe. In this picture, the bright radio structure extending from the NML into the northern giant lobe on larger scales could be interpreted as continued outflow of recently accelerated electrons, although this would have to extend to 100-kpc scales to fully explain the peculiar spectra of lobe regions 1 and 2. The strong differences in the polarization structures of the giant lobes (Cooper et al. 1965; Junkes et al. 1993), and in particular the fact that the northern giant lobe is strongly polarized with the magnetic field direction aligned along the long axis of the NML, support this picture, as do differences in the fine structure of the radio emission in the northern and southern giant lobes (Feain et al., in preparation).

If this is the case, then the spectral ages derived for the southern giant lobe (where there is no evidence of a connection to the energy supply) allow us to suggest that the last acceleration of the electrons now dominating the synchrotron radiation in this region took place around $3 \times 10^7$ yr ago (with the usual large systematic uncertainties due to the assumption of equipartition). This does not seem unreasonable given that various estimates of the dynamical age of the inner lobes give a few $\times 10^6$ yr. The dynamical age of the giant lobes, if they have expanded at speeds of the order of the sound speed in the hot external medium, with $kT \sim 0.35$ keV (Kraft et al. 2003), is expected to be almost an order of magnitude higher, but this is consistent if we assume that high-energy particles continued to be supplied to the southern giant lobe by a (now dissipated) jet throughout its lifetime.

## 6 PROSPECTS FOR INVERSE-COMPTON DETECTIONS

The mixed results on the spectra of the giant lobes imply ambiguous prospects for inverse-Compton detections at high energies. We estimate the inverse-Compton spectrum for an equipartition magnetic field using the code of Hardcastle, Birkinshaw & Worrall (1998), taking the flux densities of the giant lobes to be the sum of the fluxes for regions 1 and 2 (north lobe) and 4 and 5 (south lobe) in Table 1, and treating the lobes as cylinders in the plane of the sky. We then use two reference models for the electron energy spectrum: a J–P spectrum with a spectral age of $3 \times 10^7$ yr, as found for regions 4 and 5, for the south lobe, and a broken power law, which provides a better fit to regions 1 and 2, for the north lobe.

The energetically dominant photon population, and therefore the population that dominates the inverse-Compton luminosity, is provided by the CMB. At the large distances of the Cen A giant lobes, the energy density in photons provided by the host galaxy of Cen A is negligible, and we do not include it in our calculations; if any inverse-Compton emission arises from scattering of the galactic photons, it will preferentially be seen at small distances from the nucleus and will be hard to resolve from the nuclear high-energy emission. However, as Georganopoulos et al. (2008) have shown, the ubiquitous extragalactic background light (EBL) provides a second photon population that must be taken into account in high-energy inverse-Compton calculations. The spectral energy distribution of the EBL is not well known (indeed, Georganopoulos et al. propose inverse-Compton observations as an additional constraint on its properties) and so we must adopt a model to make a prediction. We base our estimates of EBL-related inverse-Compton emission on the spectral energy distribution[6] derived by Raue & Mazin (2008): this, while not a complete model, is intended to be consistent with all the existing direct and indirect limits. The model we use is significantly lower in photon energy density at all wavelengths than the upper range of the models adopted by Georganopoulos et al. (2008) and taken from Mazin & Raue (2007). Our inverse-Compton code includes an approximation to the Klein–Nishina correction to the effective cross-section of the electron, since these effects start to become significant when the highest-energy photons in the EBL model (which cuts off at $\lambda = 0.1$ μm) are scattered by the highest-energy electrons in the lobes, and also account for the kinematical upper limit on the energy of scattered photons (i.e. $h\nu < \gamma m_e c^2$). Since these calculations are only approximate, the results at the very highest energies should be taken as indicative only.

The results of our calculations are shown in Fig. 7. For the south giant lobe, where the J–P spectrum is used, we see a sharp cut-off in the CMB inverse-Compton prediction between about $10^{21}$ and $10^{22}$ Hz (4–40 MeV). This is as expected, since in the J–P spectrum there are no electrons above $\sim 3 \times 10^{11}$ eV (corresponding to $\gamma = 6 \times 10^5$) and significant depletion of the spectrum below that and

[6] See also http://www.desy.de/~mraue/ebl/.

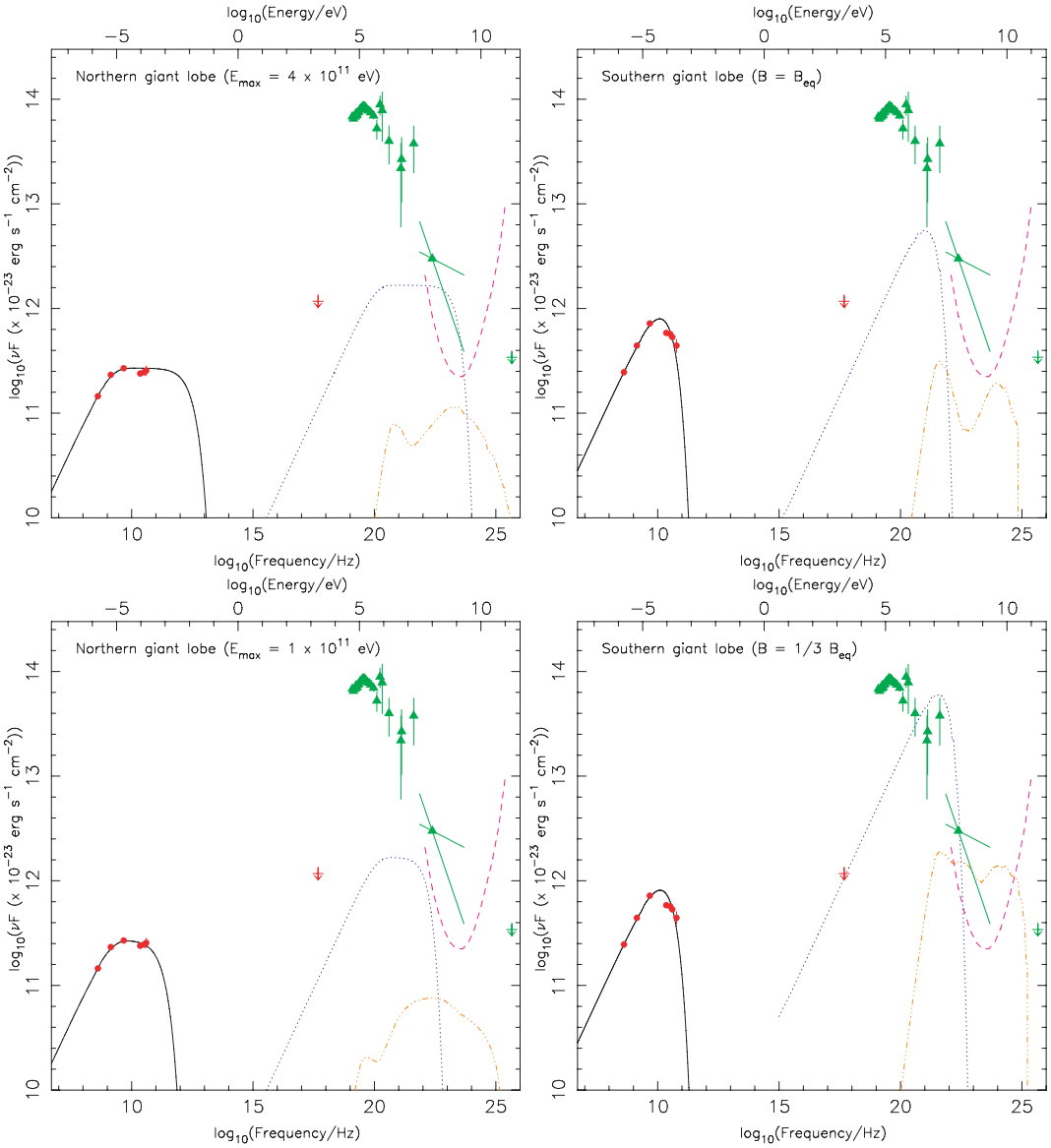


**Figure 7.** Inverse-Compton predictions for the giant lobes of Cen A. Radio data points are the sum of our measurements from the ground-based radio maps and *WMAP* data for the regions corresponding to the northern (left-hand side) and southern (right-hand side) giant lobes as described in the text. High-energy data points are the same for all panels: the soft-X-ray limit of Marshall & Clark (1981) is converted to a flux density at 2 keV ($\sim 5 \times 10^{17}$ Hz) on the assumption that $\alpha = 0.5$. The 0.05–30 MeV ($\sim 10^{19}$–$5 \times 10^{22}$ Hz) points are the reported *CGRO* OSSE and COMPTEL detections of Cen A (Steinle et al. 1998), obtained from the NASA Extragalactic Database (NED), while the bow-tie plot centred on 100 MeV is the EGRET spectrum reported by Sreekumar et al. (1999), and the point at 190 GeV ($5 \times 10^{25}$ Hz) represents the upper limit reported by Aharonian et al. (2005) from HESS observations, converted to a flux density by assuming power-law emission with photon index 3. We treat the high-energy data points as strict upper limits on the emission from the giant lobes. We also plot an estimate of the point-source *Fermi* sensitivity after 1 yr (dashed line). The solid line shows the predicted synchrotron emission for the specified electron spectrum, the dotted line shows the inverse-Compton prediction for CMB photons and the dot–dashed line shows the prediction for scattering of the EBL. For the northern giant lobe, we plot the synchrotron and inverse-Compton spectra corresponding to a broken power-law electron energy spectrum with two possible high-energy cut-offs, $4 \times 10^{11}$ eV (upper panel) and $1 \times 10^{11}$ eV (lower panel), as discussed in the text. For the southern giant lobe (right-hand panel), we plot the synchrotron spectrum and inverse-Compton predictions for a J–P model as described in the text, with the upper panel showing the predictions for an equipartition magnetic field and the lower panel those for a field strength a factor of 3 below equipartition.

the gain in energy for the inverse-Compton process is of the order of $\gamma^2$. Thus, we do not predict a *Fermi* detection for equipartition field strengths for the south giant lobe, either via CMB photons or the EBL (Fig. 7, upper right-hand panel).

On the other hand, for the broken power-law spectrum used to model the north giant lobe, the maximum energy of the electrons is unconstrained. If we were arbitrarily to assume a sufficiently large value ($\gtrsim 10^{13}$ eV), we would obtain a spectrum from scattering of the CMB that does not cut off even in the *Fermi* band ($10^{22}$–$10^{25}$ Hz). However, the predicted spectrum would be inconsistent with the 30 MeV–2 GeV EGRET detection of Cen A (Hartman et al. 1999; Sreekumar et al. 1999). The derived EGRET position

is coincident with the nucleus, so we can treat this measured spectrum, particularly at low energies, as a strict upper limit on the spectrum of either of the giant lobes, since the angular resolution of EGRET is $\sim 1^\circ$ or greater at these energies (see e.g. fig. 1 of Funk et al. 2008). If we adopt a lower value of $E_{\rm max}$, $\sim 4 \times 10^{11}$ eV, we obtain an inverse-Compton spectrum that does not violate the EGRET limit but still allows a detection of scattered CMB photons[7] of emission from this process at the extreme soft end of the *Fermi* band. This $E_{\rm max}$ is the one used in Fig. 7 (upper left-hand panel). Although still lower values of $E_{\rm max}$ are possible, it cannot be reduced too much before it starts to predict a (unobserved) high-frequency cut-off in the synchrotron spectrum. However, values of $\sim 10^{11}$ eV are permitted by the data, and this predicts no emission in the *Fermi* band (Fig. 7, lower left-hand panel). Again, neither of these models predicts strong emission from inverse-Compton scattering of the EBL in the *Fermi* band if it is close to the level of our adopted model, although it would be detected in the most sensitive part of the band if its level were close to the upper value used by Georganopoulos et al. (2008).

The inverse-Compton calculation in Fig. 7 assumes equipartition, while in general we find in the lobes of FRIIs that the observed inverse-Compton emission exceeds the equipartition prediction by a factor of a few (e.g. Croston et al. 2005). Reducing the magnetic field strength increases both the number density of electrons (since the synchrotron emissivity is fixed) and their maximum energy (since the observed cut-off frequency is fixed). However, the existing observations, particularly the soft X-ray limit of Marshall & Clark (1981), constrain the magnetic field to be no more than a factor of $\sim 3$ below equipartition. If we reduce the magnetic field by this factor, then the inverse-Compton prediction implies detectability at very soft energies of the scattered CMB even for the southern giant lobe (Fig. 7, lower right-hand panel), although we emphasize that *Fermi*-LAT observations are challenging in this energy range due to the decreased effective area and an increase in the background diffuse emission. In addition, we expect to see quite significant, spectrally distinct emission from inverse-Compton scattering of the EBL. This prediction may already marginally conflict with the *CGRO* data, and more extreme electron-density excesses over the equipartition values are certainly ruled out by both the Marshall & Clark limit and the *CGRO* spectrum, but we can conclude that even for the southern giant lobe there is a region of parameter space with $B < B_{\rm eq}$ where a *Fermi* detection is possible.

The results to be expected from *Fermi* therefore depend sensitively on the magnetic field strength in the lobes and on the unknown high-energy electron spectral cut-off in the north giant lobe. Fig. 7 illustrates some of the possibilities. If the magnetic field strength is significantly below equipartition, or if the high-energy cut-off is high enough in the north lobe, then we expect a *Fermi* detection of scattered CMB photons for our adopted sensitivities, although in all cases the *Fermi* emission must be very soft to avoid violating the limits imposed by EGRET between 30 MeV and 1 GeV. If *Fermi* does detect the giant lobes, then we will measure the magnetic field strength, and the sensitivities are such that we should be able to observe in the *Fermi* spectrum the difference in the high-energy electron spectra of the two giant lobes implied by the *WMAP* data: the resulting constraints on the magnetic field strength will then allow a measurement of, or limit on, the spectral energy density of the background of photons at higher energies (e.g. from the EBL) in the lobes. If extended inverse-Compton emission is not detected, then *Fermi* will set field-dependent limits on the high-energy cut-off in electron energies in the northern giant lobe and will improve significantly on the existing limits on magnetic field strength, but the problem of detecting inverse-Compton emission from Cen A, and thus *measuring* the magnetic field strength in the giant lobes, will remain unsolved.

[7] We use *Fermi* 1-yr $5\sigma$ point-source sensitivities taken from http://www-glast.slac.stanford.edu/software/IS/glast_lat_performance.htm: these are appropriate fiducial values in the absence of observational constraints on *Fermi*'s real performance for an extended source. Below 100 MeV, the background is expected to be high and our extrapolation is based on the sensitivity curve for the 'inner galaxy' presented in Funk et al. (2008).

## 7 UHECRs FROM THE GIANT LOBES AND THEIR POSSIBLE RADIATIVE SIGNATURES

### 7.1 Introduction

As mentioned in Section 1, at least four of the 27 PAO UHECR events in the energy range $E_{\rm p} \sim (0.6\text{–}0.9) \times 10^{20}$ eV (Abraham et al. 2007; Abraham et al. 2008) may be associated with Cen A (e.g. Moskalenko et al. 2008). Although evidence has been presented that the UHECRs include some heavier nuclei as well as protons (e.g. Unger et al. 2007), the level of uncertainty in the composition does not affect our order of magnitude estimates if, as we assume hereafter, all the events are identified with protons. In this section, we argue that the giant lobes of Cen A may confine such extremely relativistic protons, and may indeed be the sites for their acceleration. Our spectral analysis of the giant lobes suggests that there is a continuous particle (electron) acceleration in the northern part of the source, requiring, in turn, the presence of magnetic turbulence which can energize different cosmic ray species via stochastic particle–wave interactions. In addition, the parameters of the giant radio lobes of Cen A estimated in the previous sections allow us to consider the problem of acceleration of UHECRs in Cen A in a more quantitative way than has previously been possible.

### 7.2 Acceleration of UHECRs

The Larmor radius of a cosmic ray with energy $E_{\rm p} \equiv E_{20} 10^{20}$ eV gyrating in a magnetic field with intensity $B \equiv B_{-6}\, 10^{-6}$ G is $r_{\rm L} = E_{\rm p}/eB \sim 100\, E_{20} B_{-6}^{-1}$ kpc. Thus, the giant lobes of Cen A, with an estimated equipartition magnetic field $B_{-6} \sim 1$ and a spatial scale $R \sim 100$ kpc, satisfy the standard Hillas (1984) criterion for a possible source of UHECRs, since $r_{\rm L} \leq R$ for $E_{20} \leq 1$. The lobes of radio galaxies are highly magnetized, rarified cavities inflated by jets in the surrounding medium, and are expected to contain a predominantly tangled magnetic field component with the maximum wavelength of the turbulent modes possibly as large as the scale of the system. Since the giant lobes are plausibly close to equipartition between magnetic field and particle energy density, as indicated by our analysis in Sections 5 and 6, the velocities of such modes are expected to be very close to the speed of light. These are excellent conditions for the efficient stochastic acceleration of protons injected by the jets into, and confined within, the lobes, by means of resonant *Fermi*-type processes. The shortest possible time-scale for such acceleration corresponds to Bohm-type diffusion (where the particle mean-free path is comparable to the particle gyroradius:

we assume this time-scale in what follows), and is roughly[8] $t_{\rm acc} \sim 10\, r_{\rm L}/c$. This implies that

$$t_{\rm acc} \sim 3.5\, E_{20}\, B_{-6}^{-1}\ {\rm Myr}, \quad (1)$$

which is comfortably smaller than the age of the lobes estimated in the previous section, $t_{\rm lobe} \sim 30$ Myr. On the other hand, the characteristic time-scale for the diffusive escape of particles from the lobes is of the same order or longer only if $E_{20} \leq 1$, namely

$$t_{\rm diff} \sim 3\, R^2/r_{\rm L}c \sim 0.9\, R_{100}^2\, E_{20}^{-1}\, B_{-6}\ {\rm Myr}, \quad (2)$$

where $R_{100} \equiv R/100$ kpc. The maximum energy of cosmic rays available in the acceleration scenario we are considering, given by the condition $t_{\rm acc} \sim t_{\rm diff}$ (since all the other loss time-scales are much longer than $t_{\rm diff}$; see below), is $E_{20} \sim 0.5\, B_{-6}\, R_{100}$ (thus satisfying the Hillas criterion, since the condition $t_{\rm acc} \sim t_{\rm diff}$ reduces exactly to $r_{\rm L} \sim R$ for the assumed acceleration and diffusion time-scales). For the estimated lobe parameters $B_{-6} \sim 1$ and $R_{100} \sim 1$, this maximum energy is in very good agreement with the observed energies of the PAO events associated with Cen A (see above).

We next consider whether Cen A is powerful enough to account for the detected flux of UHECRs. We begin by estimating the energetics of the giant lobes assuming rough equipartition between the magnetic field, relativistic electrons and (not necessarily relativistic) protons. For a cylindrical volume matching the giant radio structure with $V = \pi R^2 h \sim 5.5 \times 10^{71}\, R_{100}^2\, h_{600}$ cm$^3$ (the radius $R \equiv R_{100}\, 100$ kpc and height $h \equiv h_{600}\, 600$ kpc), $E_{\rm tot} \sim 3\, U_{\rm B}\, V \sim 6.6 \times 10^{58}\, B_{-6}^2\, R_{100}^2\, h_{600}$ erg, where $U_{\rm B} \equiv B^2/8\,\pi \sim 4 \times 10^{-14}\, B_{-6}^2$ erg cm$^{-3}$ is the magnetic energy density. This leads to a very rough limit to the power of the jets supplying energy to the lobes

$$L_{\rm j} \sim E_{\rm tot}/2\, t_{\rm lobe} \sim 3.5 \times 10^{43}\, B_{-6}^2\, R_{100}^2\, h_{600}\ {\rm erg\,s^{-1}}. \quad (3)$$

This estimate should be considered as a lower limit, as it neglects any mechanical work done by the jets on the surrounding medium and the actual jet lifetime may also be substantially shorter than the age of the giant lobes; however, it is of the same order of magnitude as kinetic power estimates for the jets powering the inner lobes of Cen A (see Kraft et al. 2003) and with jet power estimates for more distant FRI radio galaxies (e.g. Laing & Bridle 2002). The UHECR flux detected by PAO from a point source with $N$ associated events above $E_{\rm th} = 60$ EeV energies, assuming a power-law form of the cosmic ray spectrum with a energy index $s = 2$, is $F_{\rm UHE} \sim 0.33 \times 10^{17}\, N\, E_{20}^{-2}$ km$^{-2}$ yr$^{-1}$ eV$^{-1}$, when corrected for the relative exposure appropriate for Cen A's declination (e.g. Cuoco & Hannestad 2008). The particle energy index $s$ is poorly known in the energy range we are considering; for simplicity, we assume hereafter the standard value of $s = 2$, consistent with the electron injection spectrum within the giant lobes of Cen A used in our analysis, which results in equal power stored per decade of cosmic ray energy. For $N = 4$, the monochromatic particle energy flux is then $[E_{\rm p}^2 F]_{\rm UHE} \sim 0.66 \times 10^{-12}$ erg cm$^{-2}$ s$^{-1}$ and the monochromatic particle luminosity is thus

$$L_{\rm UHE} \sim 4\pi d^2\, \left[E_{\rm p}^2 F\right]_{\rm UHE} \sim 10^{39}\ {\rm erg\,s^{-1}}. \quad (4)$$

[8] In general, we can write $t_{\rm acc} = r_{\rm L}/\eta c$, where the factor $\eta$ accounts for less than ideal efficiency of particle acceleration (see e.g. Aharonian et al. 2002). In the specific case of stochastic acceleration by magnetic turbulence (e.g. Stawarz & Petrosian 2008), the acceleration time-scale [in the Bohm limit and with a turbulence spectrum $W(k)$ going as $k^{-1}$] is given by $t_{\rm acc} = (v_{\rm A}/c)^{-2}(U_0/U_{\rm turb})\ (r_{\rm L}/c)$ where $v_{\rm A}$ is the Alfvén speed and $U_0/U_{\rm turb}$ is the ratio of energy densities in the unperturbed magnetic field and the turbulent magnetic component. Thus, for relativistic strong turbulence ($v_{\rm A} \lesssim c, U_{\rm turb} \lesssim U_0$), we expect the factor $1/\eta \sim 10$.

Even if we extrapolate the cosmic ray spectrum down to the lowest energies with $s = 2$, the total cosmic ray luminosity is found to be $L_{\rm tot} \sim 10\, L_{\rm UHE} \sim 10^{40}$ erg s$^{-1}$, and thus it constitutes a negligible fraction ($\lesssim$0.1 per cent) of the power supplied by the jets to the giant lobes.

### 7.3 Radiative signatures

As discussed in the previous section, the time-scales and energetics are both consistent with the hypothesis that UHECRs are accelerated continuously within the giant lobes of Cen A. In this scenario, the ultrarelativistic protons within the extended and magnetized lobes will radiate, with the main loss processes being due to synchrotron radiation and proton–proton (p–p) interactions.[9] The former process is characterized by a time-scale

$$t_{\rm syn} \sim 1.4 \times 10^6\, E_{20}^{-1}\, B_{-6}^{-2}\ {\rm Myr} \quad (5)$$

resulting in a synchrotron continuum peaking at photon energies $\varepsilon_{\rm syn} \sim 25\, E_{20}^2\, B_{-6}$ keV (Aharonian 2002). In the latter case, the characteristic time-scale is

$$t_{\rm pp} \sim 1.7 \times 10^6\, n_{-4}^{-1}\ {\rm Myr}, \quad (6)$$

where $n_{\rm th} \equiv n_{-4}\, 10^{-4}$ cm$^{-3}$ is the number density of the cold gas within the giant lobes, and $\gamma$-rays with energies $\varepsilon_\gamma \leq 10$ EeV for the maximum proton energy $E_{\rm p} \sim 10^{20}$ eV will be generated (see e.g. Aharonian 2002).

It follows immediately from the above results (equations 2, 4, 5) that the synchrotron emission of the cosmic ray protons produced within Cen A's giant lobes is negligible, since it is expected to peak around photon energies $\sim$10 keV with a luminosity of the order of

$$L_{\rm syn} \sim L_{\rm UHE}\, t_{\rm diff}/t_{\rm syn} \sim 10^{33}\, R_{100}^2\, B_{-6}^3\ {\rm erg\,s^{-1}}. \quad (7)$$

This is orders of magnitude below the expected X-ray luminosity of the giant lobes' electrons due to inverse-Comptonization of the CMB photon field for $B_{-6} \sim 1$ ($\sim 2 \times 10^{41}$ erg s$^{-1}$), and large increases in the magnetic field strength over the equipartition value would be required for the proton synchrotron emission to become dominant.

The expected $\gamma$-ray emission from p–p interactions might, however, be somewhat more promising in terms of allowing an independent detection of the high-energy protons. We first note that the time-scale for the diffusive escape of cosmic ray protons from the system becomes longer than the time-scale for p−p interactions below energies $E_{\rm p} \sim 100\, R_{100}^2\, B_{-6}\, n_{-4}$ TeV. Thus, all of the power channelled to such particles in the acceleration process during the lifetime of the source is released as $\gamma$-ray emission, below photon energies $\varepsilon_\gamma \sim 10$ TeV, with an expected photon index

[9] UHECR will also interact with the photon field within the lobes, via both photo-meson production and Bethe–Heitler pair production. The key quantity for the former process is the number density of photons with energies above the photo-meson production energy threshold, 300 MeV in the proton rest frame, which correspond to an observed photon energy $\varepsilon^\star = 3\, E_{20}^{-1}$ meV, or a frequency $\nu^\star = 7 \times 10^{11} E_{20}^{-1}$ Hz (Aharonian 2002). However, for $E_{20} \sim 1$, the numerically dominant photon field in the Cen A lobes around and above $\nu^\star$ (by a very large factor) is the CMB, and it is well known (e.g. Greisen 1966) that the loss time-scale is $>10^7$ yr even for $E_{20} \sim 1$, and much larger for lower energies. Although the number density of synchrotron photons available for pair production for a given UHECR energy is higher (because of the lower energy threshold for pair production), CMB photons are still numerically dominant and we know that pair production is negligible compared to photo-meson production when CMB losses are considered. We therefore neglect these loss processes in what follows.

$\Gamma_\gamma = s$ (Kelner, Aharonian & Bugayov 2006). Unfortunately, the number density of thermal protons within the lobes of radio galaxies is not known. The lack of observed internal depolarization in low-frequency radio observations (Cioffi & Jones 1980) has been used to set temperature-independent limits of the order of $10^{-4}$ cm$^{-3}$ for extended components of other radio sources (e.g. Eilek et al. 1984; Spangler & Sakurai 1985), but this method depends on assumptions about the field geometry (Laing 1984) and in any case the required multifrequency radio polarization observations of Cen A are not available to us. Isobe et al. (2001) claim an *ASCA* detection of soft X-ray emission coincident with the outer part of the giant lobes, with $kT = 0.62$ keV: assuming an abundance of 0.1 solar, we find that their quoted soft X-ray (0.5–2.0 keV) flux corresponds to a density $n_{\rm th} = 1.6 \times 10^{-4}$ cm$^{-3}$ if it comes from a uniform thermal plasma internal to the lobe. This is a strict upper limit on the gas density since emission may also be coming from gas external to the giant lobes (increasing the abundance reduces the derived density). Similarly, the Marshall & Clark (1981) 2–10 keV flux limit acts as a strict upper limit on the density of hot ($kT = 2.5$ keV) gas in the giant lobes, giving $n_{\rm th} \sim 1.3 \times 10^{-4}$ cm$^{-3}$ if all the emission comes from a uniform thermal plasma with the same abundance. These limits on densities look comparable to the expected parameters of the intergalactic medium at 100-kpc distances from the centre of the galaxy group hosting Cen A (i.e. from the Cen A host galaxy), and hence we assume $n_{-4} \sim 1$ for illustration, although we note that gas with this density must be relatively cold if it is not to dominate the energy density of the giant lobes.

With this value of $n_{-4}$, and with the model cosmic ray spectrum $s = 2$ anticipated above and normalized to the PAO flux, the expected monochromatic $\gamma$-ray luminosity from p–p interactions emitted over the whole volume of the extended giant lobes at photon energies $\leq$10 TeV is

$$L_\gamma \sim L_{\rm UHE}\, t_{\rm lobe}/t_{\rm pp} \sim 10^{34}\, n_{-4}\, {\rm erg\,s^{-1}}\,, \quad (8)$$

corresponding to a monochromatic (e.g. 10 TeV) flux energy density of only $[\varepsilon S(\varepsilon)]_\gamma \sim L_\gamma/4\pi d^2 \sim 10^{-17}\,{\rm erg\,cm^{-2}\,s^{-1}}$. This can be compared with the upper limit set on the TeV emission from the nucleus of Cen A by the existing 4.2-h High Energy Stereoscopic System (HESS) observation, $F(>0.19\,{\rm TeV}) < 5.68 \times 10^{-12}$ ph cm$^{-2}$ s$^{-1}$ (Aharonian et al. 2005; cf. Fig. 7), which, with a $\gamma$-ray photon index $\Gamma_\gamma = 2$, corresponds to a monochromatic luminosity of $[\varepsilon L(\varepsilon)]_{0.19\,{\rm TeV}} < 2.8 \times 10^{39}$ erg s$^{-1}$, or a flux of $1.7 \times 10^{-12}$ erg cm$^{-2}$ s$^{-1}$. Thus, it seems that the expected $\gamma$-ray luminosity is much below the sensitivity limit of any current TeV instrument. Note that in addition the angular resolution of HESS in the 0.1–100 TeV photon energy range is $\lesssim 0.^\circ1$, which is much better than the $\sim 10^\circ - 1^\circ$ point spread function of EGRET (Section 6) in the photon energy range $\sim$0.03–1 GeV. Cen A therefore does not appear point-like to HESS, whereas it is effectively point-like at least at low energies with EGRET, so that the sensitivity limit of HESS appropriate for an extended source will be substantially higher than the quoted point source value.

On the other hand, the estimated TeV flux of $\sim 10^{-17}$ erg cm$^{-2}$ s$^{-1}$ should be considered as a very conservative lower limit. This is because we have assumed a rather flat cosmic ray spectrum within the whole proton energy range. For any more realistic (steeper) spectrum for the accelerated cosmic rays at the highest energy range, the expected $\gamma$-ray flux increases. For example, assuming $s = 2.7$ (as used by other authors) above some break energy $E_{\rm br} < E_{\rm th}$, and $s = 2$ below $E_{\rm br}$, we obtain the PAO flux at $E_{\rm p} > E_{\rm th}$ with $N = 4$ events equal to

$$\left[E_{\rm p}^2 F\right]_{\rm UHE} \sim 1.1 \times 10^{-12}\,(E_{\rm p}/60\,{\rm EeV})^{-0.7}\,{\rm erg\,cm^{-2}\,s^{-1}} \quad (9)$$

(see Cuoco & Hannestad 2008), and thus the monochromatic cosmic ray luminosity $L_{\rm CR} \sim 1.8 \times 10^{39}\,(E_{\rm br}/60\,{\rm EeV})^{-0.7}$ erg s$^{-1}$ at proton energies $E_{\rm p} < E_{\rm br}$. For example, with $E_{\rm br} \sim 10^{18}$ eV (see in this context Kachelriess et al. 2008), one obtains $L_{\rm CR} \sim 3.2 \times 10^{40}$ erg s$^{-1}$, which is more than one order of magnitude higher than our previous estimate, resulting in an expected monochromatic $\gamma$-ray energy flux at photon energies $\leq$ 10 TeV of the order of $[\varepsilon S(\varepsilon)]_\gamma \sim 3 \times 10^{-16}\,{\rm erg\,cm^{-2}\,s^{-1}}$. Yet another reason why this is a conservative lower limit is that the re-processing of higher-energy $\gamma$-rays, produced by the $E_{\rm p} > 100$ TeV protons, has not been taken into account in our analysis, and this may increase the expected $\gamma$-ray flux by a factor of at least a few. Still, in order to reach the sensitivity limit of modern Cherenkov telescopes, the total power channelled to the cosmic rays with energies $E_{\rm p} \leq 100$ TeV would have to be of the order of 10 per cent of the total jet power, $L_{\rm CR} \sim 0.1\,L_{\rm j}$, corresponding to a total energy stored in cosmic rays from the lobes of $E_{\rm CR} \sim 10^{58}$ erg.

The possibility of detecting the high-energy $\gamma$-ray emission from p–p interactions in the giant lobes of Cen A, even though not particularly supported by our analysis presented above, is an exciting one and worth some attention, since the large extent of these lobes means that they can be resolved at the highest TeV $\gamma$-ray energies using HESS. In this way, the contribution from the inner regions of Cen A (including the inner, sub-pc to kpc scale jet, the host galaxy and active nucleus) to the total $\gamma$-ray signal could be spatially resolved from the emission from the lobes. In this context, it is important to note that our analysis of the leptonic emission generated within the extended lobes (Section 6) indicates that we expect no significant TeV radiation produced by ultrarelativistic electrons via inverse-Comptonization of either the CMB or EBL photon fields, since the limits from synchrotron and inverse-Compton continuum indicate a cut-off in the lobes' electron spectrum around energies $E_{\rm e} \lesssim 1$ TeV, providing an effective upper limit on the energy of any inverse-Compton scattered photons (Fig. 7). Thus, if any TeV emission is detected from the giant lobes, it can be safely identified with being hadronic in origin. This is in contrast to the situation at the lower photon energy range probed by *Fermi*, which can also resolve the giant lobes from the central regions of Cen A, since the expected leptonic (inverse-Compton) emission produced from the lobes is expected to dominate at GeV photon energies over any hadronic emission.

Obviously, UHECRs can in principle be accelerated in other components of the very complex Cen A system. Indeed, models for UHECR production on the very smallest scales (around the SMBH or in the inner jet) have been considered extensively in the literature. These models are all based around the general idea that the accreting SMBHs in the centres of at least some active galaxies provide a sufficient drop in potential for such an extreme acceleration. Indeed, the electromagnetic force associated with the black hole of mass $M_{\rm BH}$ rotating with angular momentum $J$ in an external magnetic field (supported by the accreting matter) with intensity $B_{\rm nuc}$ is $\Delta V \sim J\,B_{\rm nuc}/M_{\rm BH}\,c$ (Phinney 1983). The precise value for $B_{\rm nuc}$ is not known, but it is generally expected that the nuclear magnetic field energy density cannot be higher than (and may be equal to) the energy density of the accreting matter (e.g. Ghosh & Abramowicz 1997). Thus, for an object accreting at some fraction $\eta$ of the Eddington rate,

$$B_{\rm nuc} \sim 6 \times 10^4\,\eta^{1/2}\,M_8^{-1/2}\,{\rm G}, \quad (10)$$

where $M_8 \equiv M_{\rm BH}/10^8\,{\rm M}_\odot$. The spin of SMBHs in general is also a very poorly known parameter. However, assuming the spin paradigm for efficient jet production (Blandford 1990), one can

expect SMBHs in elliptical-hosted radio galaxies to be spinning at the maximal rate, $J \sim J_{\rm max} \equiv M_{\rm BH}\, c\, r_{\rm g}$, where $r_{\rm G} = G M_{\rm BH}/c^2$ is the Schwarzchild radius of the hole (see Sikora, Stawarz & Lasota 2007). These give $\Delta V \sim 10^{18}\, \eta^{1/2}\, M_8^{1/2}$ statvolt, and therefore the maximum available energy for a test particle with charge $e$ accelerated in this potential drop is as high as

$$E_{\rm max} \sim 3 \times 10^{20}\, \eta^{1/2}\, M_8^{1/2}\ {\rm eV}. \quad (11)$$

For $M_8 \sim 1$ in Cen A (Häring-Neumayer et al. 2006; Marconi et al. 2006) and assuming an accretion efficiency of the order of $\eta \sim 0.01$ (Evans et al. 2004), this leads to $E_{\rm max} \sim 3 \times 10^{19}$ eV, in agreement with the energies of the associated PAO events. However, even in these models it is not clear where and how the involved electric circuit closes. It may close very close to the black hole, or along the edges of extended radio lobes (see e.g. Blandford 2008). In the former case, UHECR protons may indeed be generated in the inner regions of Cen A (see, in this context, Kachelriess et al. 2008); however, in the latter case, stochastic interactions with the magnetic turbulence taking place in the giant lobes, as discussed in this paper (and by others, e.g. Fraschetti & Melia 2008), or some other (though more speculative) mechanism involving reconnection of the lobes' magnetic field (see, in this context, Benford & Protheroe 2008), may mediate the particle acceleration. Irrespective of the detailed mechanism, only in the case of UHECR production in the giant lobes will there be a clear radiative signature potentially detectable at GeV-TeV photon energies, since any analogous emission produced in the inner regions of the radio galaxy, even though possibly stronger due to the richer particle and photon environment (and therefore more significant p–p interactions), will always be confused with other $\gamma$-ray 'nuclear' components (e.g. Chiaberge, Capetti & Celotti 2001), including direct emission from the inner jet, or the emission from a giant pair halo created by the re-processing of such emission (as discussed in the context of Cen A by Stawarz et al. 2006). The detection or non-detection of extended GeV-TeV emission from the giant lobes of Cen A can therefore in principle help to distinguish between these models.

## 8 SUMMARY AND CONCLUSIONS

We have presented the first high-frequency, spatially resolved study of the giant lobes of Centaurus A. We confirm recent findings (Israel et al. 2008) that the overall lobe spectra steepen at frequencies above 5 GHz, but in addition we have shown that the northern and southern giant lobes are significantly different at these high frequencies: the spectrum of the southern lobe steepens monotonically (and is steeper further from the active nucleus) whereas the spectrum of the northern lobe, after an initial steepening, remains consistent with a power law to within the limits of our data. We suggest that this indicates a real difference in the particle acceleration history of the northern and southern giant lobes, perhaps due to the influence of the poorly understood NML region.

Few FRI sources have so far been studied at radio frequencies above a few tens of GHz, with more attention having been given to the hotspots and jets of powerful FRIIs (e.g. Hardcastle & Looney 2008 and references therein). The *WMAP* data for Cen A show that it is both possible and useful to study the dynamics of FRIs with high-frequency data. The Atacama Large Millimetre Array (ALMA), in combination with current and next-generation telescopes operating at lower frequencies, will allow spectral studies of large samples of well-studied FRI radio galaxies to be carried out relatively easily. It will be interesting to compare the results of such work with the results presented here for Cen A, and in particular to search for other radio sources that show strong spectral differences between the lobes at high frequencies.

Our results also have implications for the high-energy astrophysics of Cen A. If the simplest interpretation of our spectral modelling is correct, then the southern giant lobe is a true relic with no ongoing particle acceleration, while the northern giant lobe may have an electron spectrum that extends to substantially higher energies. While *Fermi* detections of both lobes remain possible, the northern lobe is likely to be more clearly detectable, and all our *Fermi* predictions imply a relatively soft spectrum for inverse-Compton scattering of the CMB. Upper limits in the soft X-ray and from the EGRET detector on board the *CGRO* already rule out magnetic field strengths more than a factor of a few below equipartition: *Fermi* will either detect the giant lobes or substantially improve this limit.

Finally, we have shown above that the giant lobes of Cen A are potential sites for acceleration of protons to the highest observed energies, $E_{\rm p} \sim 10^{20}$ eV, although we are required to adopt the most optimistic acceleration time-scale, corresponding to the Bohm limit for the particle–magnetohydrodynamics wave interactions, in order to be efficient enough to account for the PAO UHECR flux. We have also found that in this scenario the $\gamma$-ray radiative signatures accompanying the acceleration process, resulting from the interactions of ultrarelativistic protons with the thermal gas within the lobes, can possibly be observed by Cherenkov telescopes and/or by *Fermi*, thus permitting a test of this scenario.

## ACKNOWLEDGMENTS

MJH thanks the Royal Society for a research fellowship. CCC is supported by an appointment to the NASA Postdoctoral Program at Goddard Space Flight Center, administered by Oak Ridge Associated Universities through a contract with NASA. ŁS acknowledges support by MEiN grant 1-P03D-003-29. We thank Nils Odegard for providing the *WMAP* data, Norbert Junkes for providing us with radio data from ground-based observations of Cen A, Matthieu Renard for helpful discussions of the detectability of the Cen A lobes with coded-mask high-energy instruments, Gustavo Romero and Sergey Troitsky for helpful comments on the initial version of the paper, Daniel Mazin and Martin Raue for providing us with data on the EBL spectral energy density, and an anonymous referee for valuable comments which have allowed us to make significant improvements to the paper. This research has made use of the NASA/IPAC Extragalactic Data base (NED) which is operated by the Jet Propulsion Laboratory, California Institute of Technology, under contract with NASA.

## REFERENCES

Abraham J. et al. [for the Pierre Auger Collaboration], 2007, Sci, 318, 938
Abraham J. et al. [for the Pierre Auger Collaboration], 2008, Astropart. Phys., 29, 188
Aharonian F. A., 2002, MNRAS, 332, 215
Aharonian F. A., Belyanin A. A., Derishev E. V., Kocharovsky V. V., Kocharovsky V. V., 2002, Phys. Rev. D, 66, 023005
Aharonian F. et al. [for the HESS Collaboration], 2005, A&A, 441, 465
Alexander P., Leahy J. P., 1987, MNRAS, 224, 1
Alvarez H., Aparici J., May J., Reich P., 2000, A&A, 355, 863
Arp H., 1994, A&A, 288, 738
Baars J. W. M., Genzel R., Pauliny-Toth I. I. K., Witzel A., 1977, A&A, 61, 99
Benford G., Protheroe R. J., 2008, MNRAS, 383, 663

Blandford R. D., 1990, in Courvoisier T. J.-L., Mayor M., eds, Active Galactic Nuclei. Saas-Fee Advanced Course 20. Springer, Berlin, p. 161
Blandford R. D., 2008, in Rector T. A., De Young D. S., eds, ASP Conf. Ser. Vol. 386, Extragalactic Jets: Theory and Observation from Radio to Gamma Ray. Astron. Soc. Pac. San Francisco, p. 3
Cavallo G., 1978, A&A, 65, 415
Cheung C. C., 2007, in Ritz S., Michelson P., Meegan C. A., eds, AIP Conference Proceedings Vol. 921, The First GLAST Symposium. Springer, Heidelberg, p. 325
Chiaberge M., Capetti A., Celotti A., 2001, MNRAS, 324, L33
Cioffi D. F., Jones T. W., 1980, AJ, 85, 368
Clarke D. A., Burns J. O., Norman M. L., 1992, ApJ, 395, 444
Combi J. A., Romero G. E., 1997, A&AS, 121, 11
Cooke B. A., Lawrence A., Perola G. C., 1978, MNRAS, 182, 661
Cooper B. F. C., Price R. M., Cole D. J., 1965, Aust. J. Phys., 18, 589
Croston J. H., Hardcastle M. J., Harris D. E., Belsole E., Birkinshaw M., Worrall D. M., 2005, ApJ, 626, 733
Cuoco A., Hannestad S., 2008, Phys. Rev. D, 78, 023007
de Oliviera-Costa A., Tegmark M., Gaensler B. M., Jonas J., Landecker T. L., Reich P., 2008, MNRAS, 388, 247
Eilek J. A., Burns J. O., O'Dea C. P., Owen F. N., 1984, ApJ, 278, 37
Evans D. A., Kraft R. P., Worrall D. M., Hardcastle M. J., Jones C., Forman W. R., Murray S. S., 2004, ApJ, 612, 786
Fanaroff B. L., Riley J. M., 1974, MNRAS, 167, 31P
Fargion D., 2008, Phys. Sci., 78, 045901
Feigelson E. D., Schreier E. J., Delvaille J. P., Giacconi R., Grindlay J. E., Lightman A. P., 1981, ApJ, 251, 31
Ferrarese L., Mould J. R., Stetson P. B., Tonry J. L., Blakeslee J. P., Ajhar E. A., 2007, ApJ, 654, 186
Fraschetti F., Melia F., 2008, MNRAS, 391, 1100
Funk S., Reimer O., Torres D. F., Hinton J. A., 2008, ApJ, 679, 1299
Georganopoulos M., Sambruna R. M., Kazanas D., Cillis A. N., Cheung C. C., Perlman E. S., Blundell K. M., Davis D. S., 2008, ApJ, 686, L5
Ghosh P., Abramowicz M. A., 1997, MNRAS, 292, 887
Gorbunov D., Tinyakov P., Tkachev I., Troitsky S., 2008a, JETP Lett., 87, 461
Gorbunov D. S., Tinyakov P. G., Tkachev I. I., Troitsky S. V., 2008b, preprint (arXiv:0804.1088)
Greisen K., 1966, Phys. Rev. Lett., 16, 748
Gureev S., Troitsky S., 2008, preprint (arXiv:0808.0841)
Hardcastle M. J., Looney L. W., 2008, MNRAS, 388, 176
Hardcastle M. J., Birkinshaw M., Worrall D. M., 1998, MNRAS, 294, 615
Häring-Neumayer N., Cappellari M., Rix H.-W., Hartung M., Prieto M. A., Meisenheimer K., Lenzen R., 2006, ApJ, 643, 226
Hartman R. C. et al., 1999, ApJS, 123, 79
Haslam C. G. T., Salter C. J., Stoffel H., Wilson W. E., 1982, A&AS, 47, 1
Heavens A. F., Meisenheimer K., 1987, MNRAS, 225, 335
Hillas A. M., 1984, ARA&A, 22, 425
Hinshaw G. et al., 2007, ApJS, 170, 288
Hinshaw G. et al., 2008, ApJS, in press (arXiv:0803.0732)
Isobe N., Makishima K., Tashiro M., Kaneda H., 2001, in Laing R. A., Blundell K. M., eds, ASP Conf. Ser. Vol. 250, Particles and Fields in Radio Galaxies. Astron. Soc. Pac., San Francisco, p. 394
Israel F. P., Raban D., Booth R. S., Rantakyrö F. T., 2008, A&A, 483, 741
Jaffe W. J., Perola G. C., 1973, A&A, 26, 423
Jarosik N. et al., 2003, ApJS, 145, 413
Junkes N., Haynes R. F., Harnett J. I., Jauncey D. L., 1993, A&A, 269, 29
Kachelriess M., Ostapchenko S., Tomas R., 2008, preprint (arXiv:0805.2608)
Katz-Stone D. M., Rudnick L., Anderson M. C., 1993, ApJ, 407, 549
Kelner S. R., Aharonian F. A., Bugayov V. V., 2006, Phys. Rev. D, 74, 034018
Kraft R. P., Vázquez S., Forman W. R., Jones C., Murray S. S., Hardcastle M. J., Worrall D. M., Churazov E., 2003, ApJ, 592, 129
Kraft R. P. et al., 2007, ApJ, 665, 1129
Kraft R. P. et al., 2009, ApJ, submitted
Laing R. A., 1984, in Bridle A. H., Eilek J. A., eds, Physics of Energy Transport in Radio Galaxies, NRAO Workshop no. 9, NRAO, Green Bank, West Virginia, p. 90
Laing R. A., Bridle A. H., 2002, MNRAS, 336, 1161
Mandel E., Murray S. S., Roll J. B., 2001, in Harnden F. R., Primini F. A., Payne H. E., eds, ASP Conf. Ser. Vol. 238, Astronomical Data Analysis Software and Systems X. Astron. Soc. Pac., San Francisco, p. 225
Marconi A., Pastorini G., Pacini F., Axon D. J., Capetti A., Macchetto D., Koekemoer A. M., Schreier E. J., 2006, A&A, 448, 921
Markwardt C. B., Tueller J., Skinner G. K., Gehrels N., Barthelmy S. D., Mushotzky R. E., 2005, ApJ, 633, L77
Marshall F. J., Clark G. W., 1981, ApJ, 245, 840
Mazin D., Raue M., 2007, A&A, 471, 439
Morganti R., Killeen N. E. B., Ekers R. D., Oosterloo T. A., 1999, MNRAS, 307, 750
Moskalenko I. V., Stawarz Ł., Porter T. A., Cheung C. C., 2008, ApJ, submitted (arXiv:0805.1260)
Oosterloo T. A., Morganti R., 2005, A&A, 429, 469
Page L. et al., 2003, ApJS, 148, 39
Page L. et al., 2007, ApJS, 170, 335
Phinney E. S., 1983, in Ferrari A., Pacholczyk A. G., eds, Astrophysical Jets. Reidel, Dordrecht, p. 201
Raue M., Mazin D., 2008, Int. J. Mod. Phys. D, 17, 1515
Renaud M., Gros A., Lebrun F., Terrier R., Goldwuirm A., Seynolds S., Kalemci E., 2006, A&A, 456, 389
Romero G. E., Combi J. A., Perez-Bergliaffa S. E., Anchordoqui L., 1996, Astropart. Phys., 5, 279
Rothschild R. E. et al., 2006, ApJ, 641, 801
Sikora M., Stawarz Ł., Lasota J. P., 2007, ApJ, 658, 815
Spangler S. R., Sakurai T., 1985, ApJ, 297, 84
Sreekumar P., Bertsch D. L., Hartman R. C., Nolan P. L., Thompson D. J., 1999, Astropart. Phys., 11, 221
Stawarz Ł., Aharonian F., Wagner S., Ostrowski M., 2006, MNRAS, 371, 1705
Stawarz Ł., Petrosian V., 2008, ApJ, 681, 1725
Steinle H. et al., 1998, A&A, 330, 97
Unger M., Engel R., Schüssler F., Ulrich R., [for the Pierre Auger Collaboration], 2007, Astron. Nachr., 328, 614
Wibig T., Wolfendale A. W., 2007, preprint (arXiv:0712.3403)

This paper has been typeset from a TEX/LATEX file prepared by the author.